Spatially local dissipation scaling in grid turbulence from direct numerical simulations

Yohei Nishimoto (西本洋平),[1] Koji Nagata (長田孝二),[1, a)] Tomoaki Watanabe (渡邉智昭),[1] and Yi Zhou (周 毅)[2]

[1)] *Department of Mechanical Engineering and Science, Kyoto University, Kyoto 615-8530, Japan*

[2)] *School of Energy and Power Engineering, Nanjing University of Science and Technology, Nanjing 210094, China*

(Dated: 30 March 2026)

We perform a spatially defined local analysis of the normalized turbulent kinetic energy dissipation rate, C_ε, using a direct numerical simulation (DNS) database of temporally developing grid turbulence in a periodic box. The mesh-based Reynolds numbers are $Re_M = 10\,000$ and $20\,000$. Extending recent experimental local-time analyses to a fully three-dimensional flow field, we compute both global statistics over the entire domain and local statistics over spatially defined subdomains to assess nonequilibrium behavior during decay. Second- and third-order structure functions indicate negligible intermittency effects for the present cases, consistent with the relatively low turbulent Reynolds numbers Re_λ. The local C_ε depends strongly on the local Re_λ and follows a nonequilibrium scaling, $C_\varepsilon/\sqrt{Re_0} \propto Re_\lambda^{-1}$, for both Re_M and throughout the decay, where Re_0 is the global Reynolds number. This DNS-based local scaling is consistent with wind-tunnel measurements of grid-generated turbulence when analyzed using local-time frameworks. In addition, the local Kolmogorov constant C_2, defined as the peak of the second-order structure function, increases with the local Re_λ and exhibits trends consistent with those obtained from global statistics.

[a)] Author to whom correspondence should be addressed: nagata.koji.2y@kyoto-u.ac.jp

Spatially local dissipation scaling in grid turbulence from direct numerical simulations

I. INTRODUCTION

Turbulence is ubiquitous in industrial machinery and natural flows, and understanding its dynamics and developing accurate models are essential for many engineering applications. Richardson[1] introduced the concept of an energy cascade, whereby the kinetic energy of velocity fluctuations is transferred from large-scale eddies to progressively smaller scales. This process continues down to the Kolmogorov scales, where the cascade terminates and the kinetic energy is dissipated into heat by viscous effects.

The viscous dissipation rate is defined as $\varepsilon = 2\nu\langle s_{ij}s_{ij}\rangle$, where ν is the kinematic viscosity, s_{ij} is the strain-rate tensor, and $\langle\cdot\rangle$ denotes an ensemble average. Kolmogorov[2–4] showed that, under the equilibrium assumption that the interscale energy flux balances the viscous dissipation rate, the nondimensional dissipation rate

$$C_\varepsilon = \frac{\varepsilon L}{u_{\rm rms}^3} \tag{1}$$

becomes constant, where $u_{\rm rms}$ is the root-mean-square (r.m.s.) velocity fluctuation and L is a characteristic large-eddy length scale, typically taken as the integral length scale. Seoud and Vassilicos[5] first demonstrated nonequilibrium regions in the lee of a self-similar (fractal) grid, where C_ε is not constant. Valente and Vassilicos[6] further reported that even classical grid turbulence generated by a regular rectangular grid can exhibit nonequilibrium dissipation in the initial decay region, with

$$C_\varepsilon \propto \frac{Re_0^{m/2}}{Re_\lambda^n}, \quad m, n \approx 1, \tag{2}$$

where Re_0 is a Reynolds number set by the initial conditions (often referred to as the global Reynolds number) and $Re_\lambda = u_{\rm rms}\lambda/\nu$ (λ is the Taylor microscale) is the turbulent Reynolds number. Subsequent studies confirmed similar behavior.[7] For early work on dissipation in turbulent flows, see Vassilicos.[8] Nagata et al.[9] investigated the influence of grid geometry using wind-tunnel experiments with 11 different grids and showed that geometric inhomogeneity promotes the emergence of the nonequilibrium law. From a theoretical perspective, Bos and Rubinstein[10] applied a perturbation analysis and provided a rationale for the empirical nonequilibrium scaling by deriving

$$\frac{C_\varepsilon}{C_{\varepsilon eq}} \sim \left(\frac{Re_\lambda}{Re_{\lambda eq}}\right)^{-15/14}, \tag{3}$$

where the subscript eq denotes equilibrium values.

More recently, Kitamura et al.[11] derived an exact relationship between C_ε and the integrated form of the Kármán–Howarth equation for forced and decaying homogeneous isotropic turbulence. They showed that, in decaying turbulence initialized from a forced-turbulence state, nonequilibrium dissipation can arise from an imbalance between $u_{\rm rms}$ and $\mathrm{d}L/\mathrm{d}t$, while the nonlinear energy transfer remains approximately constant. These results motivate analyses that go beyond global averaging. Indeed, Zheng et al.[12,13] performed a local analysis of hot-wire time series in static- and active-grid turbulence and found that the local (short-time-averaged) C_ε follows nonequilibrium scaling even far downstream, despite the global (long-time-averaged) C_ε being essentially independent of Re_λ. A natural extension is to apply an analogous local analysis to three-dimensional fields from direct numerical simulation (DNS), where spatially defined local subdomains can be examined directly, without invoking Taylor's frozen-turbulence hypothesis.

The appearance of the $-5/3$ scaling in turbulent energy spectra, particularly in nonequilibrium turbulence and in flows exhibiting internal or external intermittency, has also attracted interest.[14–17] Kolmogorov[2–4] proposed that, at sufficiently high Reynolds numbers, the energy spectrum in the inertial subrange can be written as

$$E(k) = C_k\,\varepsilon^{2/3}k^{-5/3}, \tag{4}$$

where $E(k)$ is the energy spectrum, C_k is the Kolmogorov constant, and k is the wavenumber. Laizet et al.[14] showed that, in grid turbulence, a power law close to $-5/3$ emerges relatively near the grid, where the velocity fluctuations are highly intermittent and strongly non-Gaussian. Zhou et al.[15–17] further reported that an extended $-5/3$ spectrum can occur in a highly intermittent flow with strong vortex shedding behind two side-by-side square cylinders. The corresponding physical-space statistic is the second-order structure function $\langle(\Delta_r u)^2\rangle$, where $\Delta_r u = u(\mathbf{x}+\mathbf{r})-u(\mathbf{x})$ and $r = |\mathbf{r}|$ is the separation distance. The Kolmogorov constant C_2 is then defined as the peak value of $\langle(\Delta_r u)^2\rangle/(\varepsilon r)^{2/3}$. Chien et al.[18] performed particle image velocimetry (PIV) measurements in oscillating-grid turbulence and found that C_2 depends on the amplitude of fluctuations in the large-scale energy input. They also

proposed a model for the Kolmogorov constants by assuming that the equilibrium relation $\varepsilon \propto u_{\rm rms}^3/L$ remains valid even in unsteady flows. More recently, Zhou et al.[19] examined the influence of external intermittency on the Kolmogorov constants C_k and C_2 in spectral and physical spaces and reported power-law dependences on the intermittency factor γ, namely $C_k \sim \gamma^{1/3}$ and $C_2 \sim \gamma^{1/3}$. These studies motivate an examination of how nonequilibrium dissipation is connected to the second-order structure function and the Kolmogorov constant C_2, particularly when local statistics exhibit nonequilibrium behavior.

This paper investigates the local scaling of C_ε using a DNS database of temporally developing grid turbulence and assesses the robustness of nonequilibrium dissipation scaling in spatially defined local subdomains. We also evaluate the Kolmogorov constant C_2 using both global and local statistics and examine its dependence on the global and local Re_λ. The DNS dataset itself and its global decay characteristics were documented in Ref. 20; here the new contribution of the present work is to examine spatially defined local statistics to assess nonequilibrium dissipation scaling without invoking Taylor's frozen-turbulence hypothesis.

The remainder of the paper is organized as follows: Sec. II describes the DNS database and the analysis procedure; Sec. III presents the results; and Sec. IV summarizes the conclusions.

II. DNS DATABASE AND ANALYSIS

A. DNS database of a temporally developing grid turbulence

The DNS database of temporally developing grid turbulence is briefly summarized below; detailed descriptions can be found in our previous paper.[20] The present DNS dataset was generated and its global decay properties were reported in Ref. 20. The flow considered here is grid-generated turbulence produced by a square mesh of size M and bar thickness $d = 0.2M$ (solidity $\sigma = 0.36$) towed at a constant velocity U_0 (see Fig. 1). The Reynolds number based on the mesh size is $Re_M = U_0 M/\nu$. Two Reynolds numbers are considered: $Re_M = 10\,000$ and $20\,000$. The governing equations are the incompressible Navier–Stokes equations.

The simulations do not resolve the explicit geometry of the turbulence-generating grid. Instead, an initial condition representing the wakes of a towed grid (in x-direction) is prescribed in a cubic computational domain of side length $L_x = L_y = L_z = l_{\rm box}$, with periodic

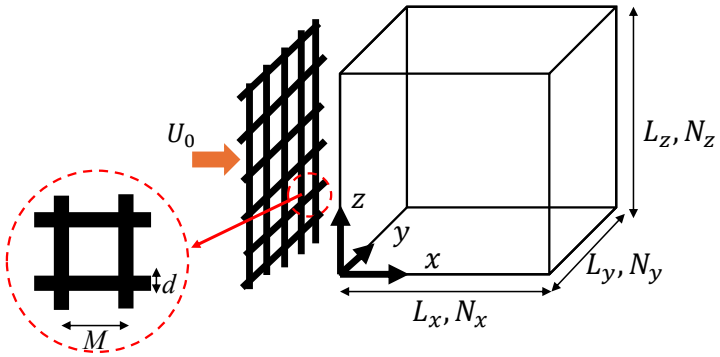

FIG. 1: Computational domain and coordinate system

TABLE I: Parameters for a temporally developing grid turbulence

Run	Re_M	l_{box}	N^3	d/M	σ	T_{end}
Re1	10 000	$20M$	2304^3	0.2	0.36	1024
Re2	20 000	$10M$	2048^3	0.2	0.36	1024

boundary conditions applied in all three directions. The simulation parameters are summarized in Table I. The total number of grid points is N^3, where $N_x = N_y = N_z = N$. The dimensionless end time T_{end} corresponds to the streamwise distance x/M in wind-tunnel experiments, where $x = tU_0$.

The initial velocity field is specified as

$$U = \langle U \rangle_x + u', \qquad V = v', \qquad W = w', \tag{5}$$

where (U, V, W) are the instantaneous velocity components in the (x, y, z) directions, and (u', v', w') denote the fluctuating components (0.5% of U_0). $\langle \cdot \rangle_x$ denotes the average taken in the x direction, represented as a function of y and z. The streamwise mean velocity $\langle U \rangle_x$ is homogeneous in the x-direction and prescribed as

$$\langle U \rangle_x = \begin{cases} U_0, & \text{behind the grid bars,} \\ 0, & \text{elsewhere.} \end{cases} \tag{6}$$

This top-hat profile approximates the velocity distribution produced by a towed grid. Then, the wakes develop into a turbulent state and merge over time, eventually forming grid turbulence. The representativeness of the present DNS configuration—a periodic domain initialized with a top-hat wake profile without explicitly resolving the grid geometry—as well as the numerical method and its validation against wind-tunnel measurements, have been examined and documented in detail in our previous study.[20] To keep the present manuscript concise and focused on the new local-scaling analysis, we therefore include here only the essential numerical information required for reproducibility and refer the reader to Ref. 20 for the full description of the methodology and validation.

B. Local scale analysis

For each case (Re1 and Re2), the computational domain is partitioned into cubic subdomains whose side length is set by the integral length scale L. This setup enables a local characterization of the dissipation scaling while retaining a subdomain size representative of the energy-containing motions. Note that the subdomains are non-overlapping.

The integral length scale is obtained from the longitudinal velocity autocorrelation by integration. Specifically, we compute the directional correlations $f_x(r) = \langle u'(x+r)u'(x)\rangle/\langle u'(x)^2\rangle$, $f_y(r) = \langle v'(y+r)v'(y)\rangle/\langle v'(y)^2\rangle$, and $f_z(r) = \langle w'(z+r)w'(z)\rangle/\langle w'(z)^2\rangle$, and define the corresponding integral scales $L_{ux} = \int_0^\infty f_x(r)\,dr$, $L_{vy} = \int_0^\infty f_y(r)\,dr$, and $L_{wz} = \int_0^\infty f_z(r)\,dr$. The integral length scale used in this study is taken as the average of the three directional values, $L = (L_{ux} + L_{vy} + L_{wz})/3$. In each case, the integral is truncated at the first separation distance r at which the corresponding $f_i(r)$ reaches zero.

We evaluate L at each time and set the subdomain side length proportional to its instantaneous value, i.e. $\ell = L(t)$, so that each subdomain contains a comparable portion of the large-scale eddies throughout the decay. In the present DNS, $L(t)$ varies by about a factor of three over the analyzed interval;[20] using a fixed ℓ would therefore lead to an $\mathcal{O}(3)$ change in $\ell/L(t)$ and would make the local averages non-uniform across time. This is consistent with the experimental procedure, where L is evaluated at each downstream position and the local analysis uses $L(x)$ (spatial evolution rather than temporal evolution).[12]

The local turbulent Reynolds number is defined as $Re_\lambda = u_{k,\mathrm{rms}}\lambda/\nu$, where both $u_{k,\mathrm{rms}}$ and λ are evaluated within each subdomain. Following our definition of the turbulent kinetic

energy $K = \frac{1}{2}\left(u_{x,\mathrm{rms}}^2 + u_{y,\mathrm{rms}}^2 + u_{z,\mathrm{rms}}^2\right)$, we define the representative (three-direction) rms velocity as

$$u_{k,\mathrm{rms}} \equiv \sqrt{\frac{2K}{3}} = \sqrt{\frac{1}{3}(u_{x,\mathrm{rms}}^2 + u_{y,\mathrm{rms}}^2 + u_{z,\mathrm{rms}}^2)},$$

with the component rms values

$$u_{x,\mathrm{rms}} = \langle u'^2 \rangle^{1/2}, \quad u_{y,\mathrm{rms}} = \langle v'^2 \rangle^{1/2}, \quad u_{z,\mathrm{rms}} = \langle w'^2 \rangle^{1/2},$$

where the spatial averages are taken over the grid points contained in the subdomain. This representative velocity $u_{k,\mathrm{rms}}$ is also used in the definition of the nondimensional dissipation coefficient, $C_\varepsilon = \varepsilon L / u_{k,\mathrm{rms}}^3$.

The Taylor microscale is calculated as

$$\lambda_j = \frac{u_{j,\mathrm{rms}}}{\sqrt{\left\langle (\partial u_j / \partial x_j)^2 \right\rangle}} \quad \text{(no summation over } j\text{)}, \quad \lambda = \frac{1}{3}\left(\lambda_x + \lambda_y + \lambda_z\right).$$

Finally, for each subdomain we compute Re_λ from the resulting subdomain-averaged $u_{k,\mathrm{rms}}$ and λ. Conditional averages are then computed by binning the subdomains according to this subdomain-based Re_λ.

In practice, the range between the minimum and maximum subdomain-averaged Re_λ values is divided into 25 logarithmically spaced bins, and ensemble averages are evaluated within each bin. A bin is deemed to have sufficient samples when the number of subdomains it contains exceeds $1/100$ of the total number of subdomains; bins with smaller sample counts are excluded from the plots to avoid large statistical uncertainty. Throughout this paper, statistics evaluated over the entire domain are referred to as "global statistics," while those evaluated over the subdomains are referred to as "local statistics."

In our previous wind-tunnel experiments,[12] we examined the sensitivity of the scaling to the choice of the local time window $T_L = C(L/u_{\mathrm{rms}})$ by varying the constant C from 0.3 to 5, and found that the scaling is essentially insensitive to C within this range. In the present study, we performed an analogous sensitivity test for the spatially defined subdomains by varying the subdomain side length from $0.5L$ to $2.0L$ (not shown). Within this range, the scaling $C_\varepsilon/\sqrt{Re_0} \sim Re_\lambda^{-1}$ remains nearly unchanged. This supports our choice of $\ell \sim L$ as a practical compromise: subdomains that are too large may smear out local variations, whereas subdomains that are too small may suffer from insufficient statistical convergence and can introduce artifacts.

III. RESULTS AND DISCUSSION

A. Global Statistics

Figure 2 shows the evolution of the nondimensional dissipation rate C_ε as a function of $(t-t_0)/t_r$. Here, t_0 is the virtual time origin determined from the velocity variance (Ref. 20), and $t_r = M/U_0$ is the reference time. This plot corresponds to Fig. 11 of Ref. 20, but here the abscissa is shifted by t_0 to facilitate comparison with experimental analyses.[9,21,22] For Re1, C_ε increases over most of the decay, reflecting the growing influence of viscous effects as the turbulence decays.[20–22] For Re2, C_ε also increases at late times ($t/t_r \gtrsim 200$), whereas it remains nearly constant over $t/t_r \approx 30$–200. Overall, the magnitude of C_ε is comparable to the experimental results reported in previous studies.[9,21,22] The relationship between C_ε and Re_λ (not shown) is consistent with previous studies; see Ref. 20.

Figure 3 shows the compensated longitudinal second- and third-order structure functions, $\langle(\Delta_r u)^2\rangle/(\varepsilon r)^{2/3}$ and $\langle(\Delta_r u)^3\rangle/(\varepsilon r)$, plotted against r/η, where $\eta = (\nu^3/\varepsilon)^{1/4}$ is the Kolmogorov length scale. The statistics are evaluated at $t/t_r = 64$ and compared with grid-turbulence measurements at similar Re_λ.[23] The present profiles agree well with those reported for grid turbulence at similar Re_λ,[23] supporting the validity of the DNS database used in this study. The peak values are substantially smaller than the high-Re_λ limits of 2 and 4/5 for the second- and third-order structure functions, respectively, reflecting finite-Re_λ effects.[23] In what follows, we define the second-order Kolmogorov constant C_2 as the peak value of $\langle(\Delta_r u)^2\rangle/(\varepsilon r)^{2/3}$.

Figure 4 shows the compensated second-order structure function at $t/t_r = 16$ and 64 as a function of r/η. The insets show $\langle\varepsilon_r^{2/3}\rangle/\varepsilon^{2/3}$, where ε_r is the dissipation rate averaged over a sphere of radius r. Note that for the pth-order structure functions,[18]

$$\langle(\Delta_r u)^p\rangle = C_p\langle\varepsilon_r^{p/3}\rangle r^{p/3} = C_p\frac{\langle\varepsilon_r^{p/3}\rangle}{\varepsilon^{p/3}}(\varepsilon r)^{p/3}\,, \tag{7}$$

where C_p is a dimensionless constant (in particular, C_2 corresponds to $p = 2$ with $C_2 = 2$ for sufficiently high Re_λ). Although $\langle\varepsilon_r\rangle$ differs from ε at small separations (small r/η) at $t/t_r = 16$, the compensated structure function is essentially unchanged over the range relevant to the peak value used to define C_2. A similar conclusion is obtained for the third-order structure function shown in Fig. 5. These results indicate that internal-intermittency effects

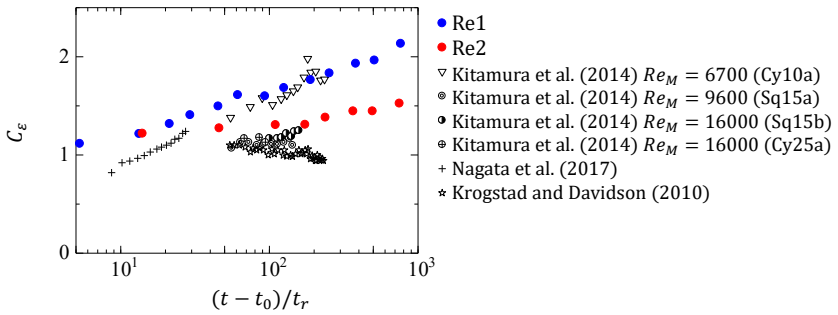

FIG. 2: Evolution of the nondimensional dissipation rate C_ε as a function of $(t-t_0)/t_r$. Experimental data[9,21,22] are included for comparison.

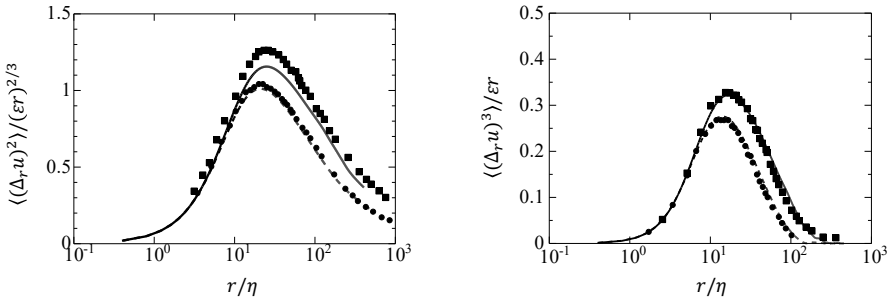

(a) (b)

FIG. 3: Compensated longitudinal (a) second-order structure function $\langle(\Delta_r u)^2\rangle/(\varepsilon r)^{2/3}$ and (b) third-order structure function $\langle(\Delta_r u)^3\rangle/(\varepsilon r)$ plotted against r/η at $t/t_r = 64$. Lines show the present DNS results and symbols indicate the measurements of Zhou and Antonia (Ref. 23) at comparable Re_λ. Dashed line: $Re_\lambda = 23$ (Re1); solid line: $Re_\lambda = 38$ (Re2); filled circles: $Re_\lambda = 27$ (Ref. 23); filled squares: $Re_\lambda = 50$ (Ref. 23).

associated with $\langle\varepsilon_r\rangle$ are negligible for the present cases, in which Re_λ remains relatively low even at early decay times. Accordingly, in the local analysis below, we evaluate C_2 using ε in $\langle(\Delta_r u)^2\rangle/(\varepsilon r)^{2/3}$.

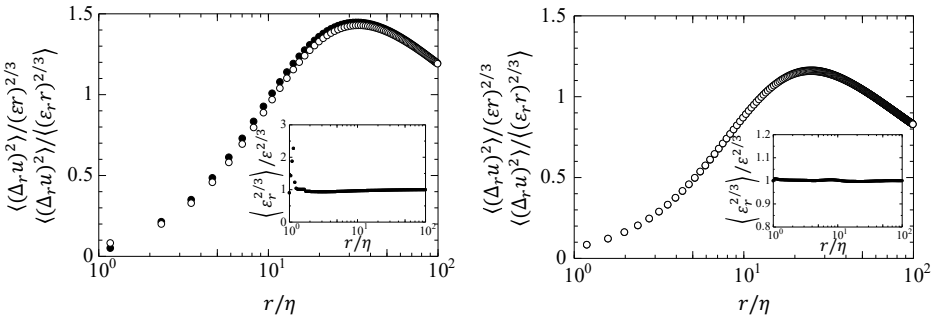

(a) (b)

FIG. 4: Compensated second-order structure function in Re2 at (a) $t/t_r = 16$ and (b) $t/t_r = 64$. Filled symbols: $\langle(\Delta_r u)^2\rangle/\langle(\varepsilon_r r)^{2/3}\rangle$; open symbols: $\langle(\Delta_r u)^2\rangle/(\varepsilon r)^{2/3}$. Insets show $\langle\varepsilon_r^{2/3}\rangle/\varepsilon^{2/3}$.

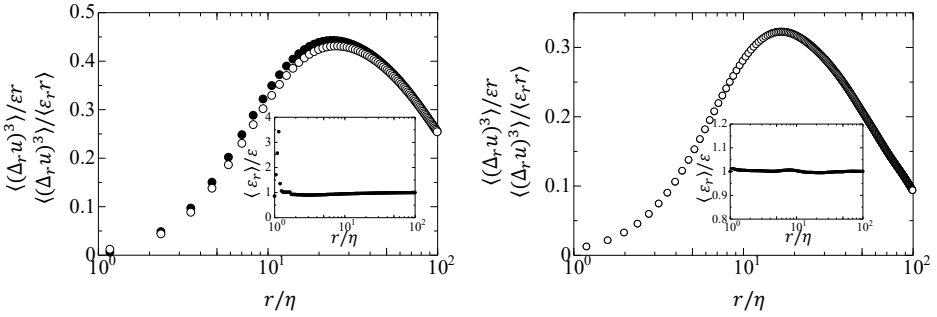

(a) (b)

FIG. 5: Compensated third-order structure function in Re2 at (a) $t/t_r = 16$ and (b) $t/t_r = 64$. Filled symbols: $\langle(\Delta_r u)^3\rangle/\langle\varepsilon_r r\rangle$; open symbols: $\langle(\Delta_r u)^3\rangle/(\varepsilon r)$. Insets show $\langle\varepsilon_r\rangle/\varepsilon$.

B. Local Statistics

To assess the nonequilibrium scaling, we normalize C_ε by $\sqrt{Re_0}$ following Eq. (2); the result is shown in Fig. 6(a). Here, Re_0 is taken as the global turbulent Reynolds number Re_λ at each t/t_r.[12] The datasets collapse well across times and both Re_M cases, and they follow the scaling $C_\varepsilon/\sqrt{Re_0} \sim Re_\lambda^{-1}$, particularly at higher Re_λ. The slight deviation at lower Re_λ

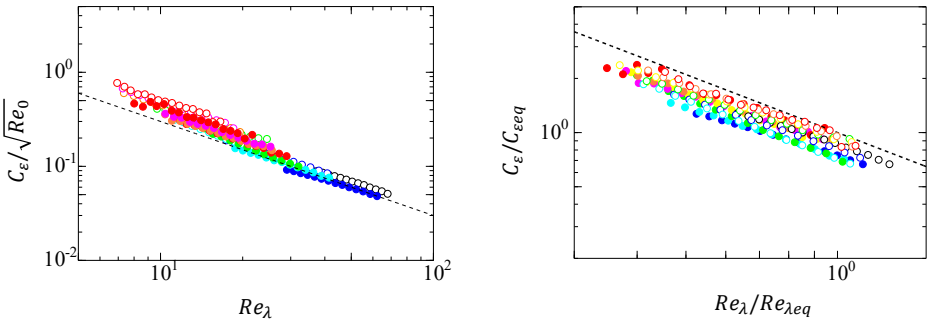

(a) (b)

FIG. 6: (a) $C_\varepsilon/\sqrt{Re_0}$ as a function of Re_λ for Re1 and Re2. The dotted line indicates the Re_λ^{-1} scaling for the global statistics. (b) $C_\varepsilon/C_{\varepsilon eq}$ as a function of $Re_\lambda/Re_{\lambda eq}$ for Re1 and Re2. The dotted line shows the prediction of Eq. (3) for the global scale. Open circles denote Re1 and filled circles denote Re2. Colors represent different times t/t_r, ranging from 8 to 512.

is likely attributable to residual viscous effects. A least-squares fit yields slopes of -0.97 for Re1, -0.96 for Re2, and -0.96 for all data. We also show $C_\varepsilon/C_{\varepsilon eq}$ versus $Re_\lambda/Re_{\lambda eq}$ [Eq. (3)] in Fig. 6(b). In the original derivation of Eq. (3), the subscript eq denotes an equilibrium value. In practice, however, equilibrium values cannot be determined; therefore, we use the global values of C_ε and Re_λ.[12] The local profiles also agree well with the nonequilibrium scaling in Eq. (3).

Finally, Fig. 7 shows the second-order Kolmogorov constant C_2 as a function of Re_λ for both global and local statistics. For the local analysis, C_2 is evaluated in each subdomain and then conditionally averaged with respect to the local value of Re_λ. For comparison, we also include results from DNS of statistically steady homogeneous turbulence[24,25] and experiments in Rayleigh–Bénard turbulent convection.[26] Consistent with the global analysis, C_2 increases with Re_λ also in the local subdomains, and the local conditioned averages follow the global trend. This indicates that, within the present parameter range, C_2 is not strongly influenced by the nonequilibrium behavior observed in C_ε.

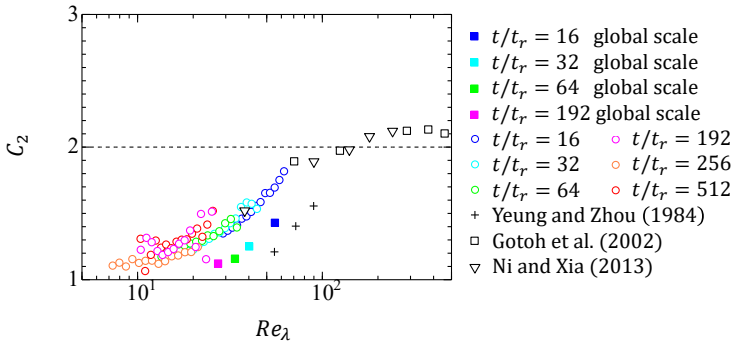

FIG. 7: Second-order Kolmogorov constant C_2 as a function of Re_λ for global and local statistics in Re2. Reference data[24–26] are included for comparison. The horizontal line indicates the high-Re_λ limit $C_2 = 2$.

IV. CONCLUSIONS

In this study, we investigated the scaling of the nondimensional dissipation rate C_ε in grid-generated turbulence using a DNS database of temporally developing turbulence initialized to mimic the wakes behind a towed grid. Two mesh Reynolds numbers, $Re_M = 10\,000$ (Re1) and $Re_M = 20\,000$ (Re2), were analyzed by comparing statistics evaluated over the whole domain (global statistics) with those evaluated over spatially defined subdomains (local statistics).

The local C_ε decreases systematically with increasing local Re_λ, indicating nonequilibrium dissipation behavior. When normalized by $\sqrt{Re_0}$, where Re_0 is the global Reynolds number at each time in two different cases, the local data collapse across times and both Re_M cases and follow the nonequilibrium scaling $C_\varepsilon/\sqrt{Re_0} \sim Re_\lambda^{-1}$, particularly at higher Re_λ.

We also evaluated the second-order Kolmogorov constant C_2 in the local subdomains. As observed at the global scale, C_2 increases with Re_λ, and the local values are consistent with the global values. This indicates that C_2 is not strongly affected by the nonequilibrium behavior of C_ε in the present flows. Furthermore, comparisons using ε_r and ε show negligible internal-intermittency effects at the present Re_λ, supporting the use of ε in the subsequent local evaluations.

Overall, the present DNS enables a spatially defined local analysis of nonequilibrium

dissipation in a fully three-dimensional flow field, thereby extending experimental local-time approaches without invoking Taylor's frozen-turbulence hypothesis. While the grid resolution is not at the absolute state of the art compared with the largest contemporary DNS (e.g., Sakurai and Ishihara[27]), it remains sufficiently large for grid-turbulence-oriented simulations and for the range of Re_λ considered here, as supported by our validation against available experimental data. The results support the view that nonequilibrium dissipation scaling is robust when assessed using local statistics. Future work should explore higher-Re_λ regimes enabled by higher-resolution simulations, as well as different initial/grid conditions, to clarify the roles of intermittency in local dissipation scaling.

ACKNOWLEDGMENTS

The authors are grateful to the anonymous reviewers for their constructive and insightful comments, which helped improve the manuscript. This work was supported by JSPS KAKENHI Grant No. JP23K22669. The authors acknowledge the financial support by Research Institute for Mathematical Sciences, Kyoto University. Y. Z. gratefully acknowledges the support of the National Science Foundation of China (No.12472223).

AUTHOR DECLARATIONS

Conflict of interest

The authors have no conflicts to disclose.

Author Contributions

Yohei Nishimoto: Data Curation (lead); Formal Analysis (lead); Investigation (equal); Methodology (equal); Validation (lead); Writing/Original Draft Preparation (lead); Writing/Review & Editing (equal). **Koji Nagata**: Conceptualization (lead); Formal Analysis (supporting); Funding Acquisition (lead); Investigation (lead); Methodology (lead); Project Administration (lead); Supervision (lead); Validation (equal); Writing/Original Draft Preparation (equal); Writing/Review & Editing (lead). **Tomoaki Watanabe**: Conceptualization (equal); Data Curation (equal); Formal Analysis (equal); Investigation (equal); Methodol-

ogy (equal); Project Administration (equal); Resources (lead); Supervision (equal); Validation (equal); Writing/Review & Editing (equal). **Yi Zhou**: Conceptualization (equal); Data Curation (supporting); Formal Analysis (supporting); Investigation (equal); Methodology (equal); Validation (supporting); Writing/Review & Editing (supporting).

DATA AVAILABILITY

The data that support the findings of this study are available from the corresponding author upon reasonable request.

REFERENCES

[1]L. F. Richardson, *Weather Prediction by Numerical Process* (Cambridge University Press, Cambridge, 1922).

[2]A. N. Kolmogorov, "Dissipation of energy in the locally isotropic turbulence," Proc. R. Soc. Lond. A **434**, 15 (1991).

[3]A. N. Kolmogorov, "On degeneration (decay) of isotropic turbulence in an incompressible viscous liquid," Dokl. Akad. Nauk SSSR **31**, 538 (1941).

[4]A. N. Kolmogorov, "The local structure of turbulence in incompressible viscous fluid for very large Reynolds numbers," Dokl. Akad. Nauk SSSR **30**, 301 (1941).

[5]R. E. Seoud and J. C. Vassilicos, "Dissipation and decay of fractal-generated turbulence," Phys. Fluids **19**, 105108 (2007).

[6]P. C. Valente and J. C. Vassilicos, "Universal dissipation scaling for nonequilibrium turbulence," Phys. Rev. Lett. **108**, 214503 (2012).

[7]R. J. Hearst and P. Lavoie, "Decay of turbulence generated by a square-fractal-element grid," J. Fluid Mech. **741**, 567 (2014).

[8]J. C. Vassilicos, "Dissipation in turbulent flows," Annu. Rev. Fluid Mech. **47**, 95 (2015).

[9]K. Nagata, T. Saiki, Y. Sakai, Y. Ito, and K. Iwano, "Effects of grid geometry on non-equilibrium dissipation in grid turbulence," Phys. Fluids **29**, 015102 (2017).

[10]W. J. Bos and R. Rubinstein, "Dissipation in unsteady turbulence," Phys. Rev. Fluids **2**, 022601 (2017).

[11]T. Kitamura, K. Nagata, K. Shimoyama, and T. Nanri, "On the normalised energy dissipation rate in homogeneous isotropic turbulence," J. Fluid Mech. **1010**, A14 (2025).

[12]Y. Zheng, K. Nakamura, K. Nagata, and T. Watanabe, "Unsteady dissipation scaling in static- and active-grid turbulence," J. Fluid Mech. **956**, A20 (2023).

[13]Y. Zheng, N. Koto, K. Nagata, and T. Watanabe, "Unsteady dissipation scaling of grid turbulence in the near-field region," Phys. Fluids **35**, 095131 (2023).

[14]S. Laizet, J. Nedić, and J. C. Vassilicos, "The spatial origin of $-5/3$ spectra in grid-generated turbulence," Phys. Fluids **27**, 065115 (2015).

[15]Y. Zhou, K. Nagata, Y. Sakai, and T. Watanabe, "Extreme events and non-Kolmogorov $-5/3$ spectra in turbulent flows behind two side-by-side square cylinders," J. Fluid Mech. **874**, 677 (2019).

[16]Y. Zhou, K. Nagata, Y. Sakai, T. Watanabe, Y. Ito, and T. Hayase, "Energy transfer in turbulent flows behind two side-by-side square cylinders," J. Fluid Mech. **903**, A4 (2020).

[17]Y. Zhou, K. Nagata, Y. Ito, Y. Sakai, and Y. Hattori, "Appearance of the $-5/3$ scaling law in spatially intermittent flows with strong vortex shedding," Phys. Fluids **35**, 045116 (2023).

[18]C. C. Chien, D. B. Blum, and G. A. Voth, "Effects of fluctuating energy input on the small scales in turbulence," J. Fluid Mech. **737**, 527 (2013).

[19]Y. Xie, X. L. Xiong, Y. Zheng, K. Nagata, T. Watanabe, and Y. Zhou, "Scaling law of the Kolmogorov constants in turbulent flow with external intermittency," J. Fluid Mech. **1019**, A30 (2025).

[20]T. Watanabe and K. Nagata, "Integral invariants and decay of temporally developing grid turbulence," Phys. Fluids **30**, 105111 (2018).

[21]P.-Å. Krogstad and P. A. Davidson, "Is grid turbulence Saffman turbulence?" J. Fluid Mech. **642**, 373 (2010).

[22]T. Kitamura, K. Nagata, Y. Sakai, A. Sasoh, O. Terashima, H. Saito, and T. Harasaki, "On invariants in grid turbulence at moderate Reynolds numbers," J. Fluid Mech. **738**, 378 (2014).

[23]T. Zhou and R. A. Antonia, "Reynolds number dependence of the small-scale structure of grid turbulence," J. Fluid Mech. **406**, 81 (2000).

[24]T. Gotoh, D. Fukayama, and T. Nakano, "Velocity field statistics in homogeneous steady turbulence obtained using a high-resolution direct numerical simulation," Phys. Fluids **14**,

1065 (2002).

[25]P. K. Yeung and Y. Zhou, "Universality of the Kolmogorov constant in numerical simulations of turbulence," Phys. Rev. E **56**, 1746 (1997).

[26]R. Ni and K. Q. Xia, "Kolmogorov constants for the second-order structure function and the energy spectrum," Phys. Rev. E **87**, 023002 (2013).

[27]Y. Sakurai and T. Ishihara, "Direct numerical simulations of compressible turbulence in a periodic box: Effect of isothermal assumptions on turbulence statistics," Phys. Fluids **36**, 085152 (2024).